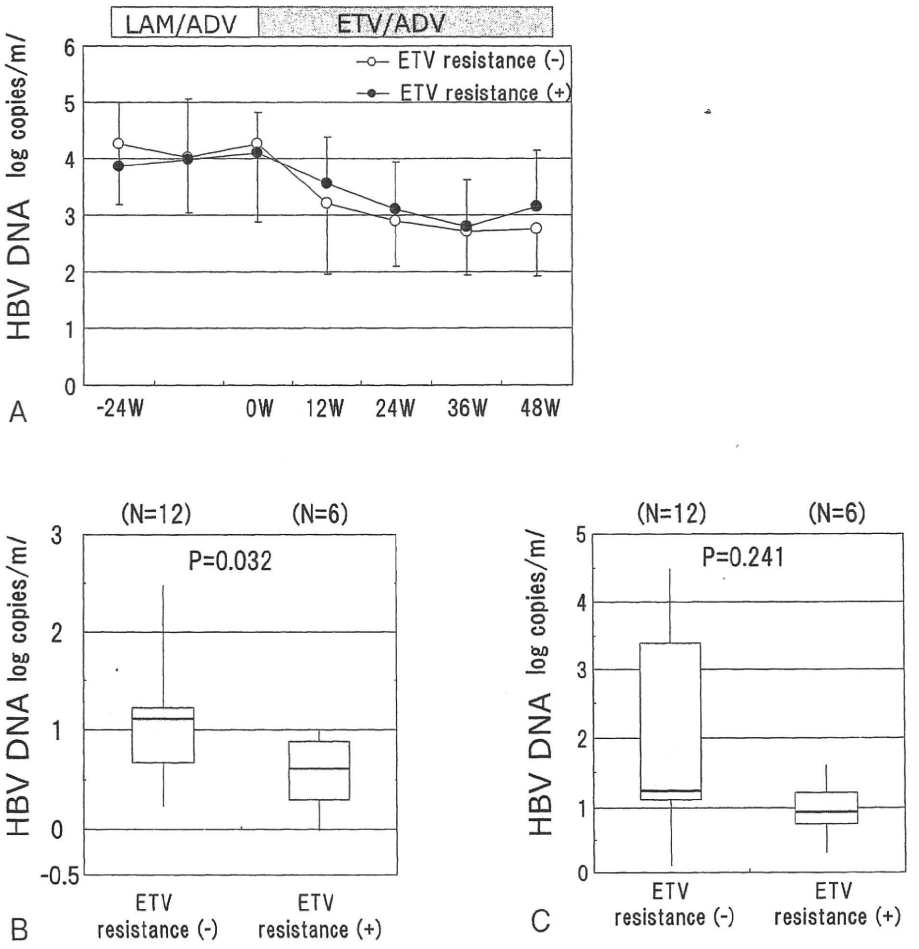

Figure 2. ETV耐性の有無によるLAM/ADV療法・ADV/ETV療法によるHBV DNAの推移 **A**）HBV DNAの推移. **B**）ADV/ETV療法ベースライン・12週後のHBV DNAの減衰量の比較. **C**）ADV/ETV療法ベースライン・48週後のHBV DNAの減衰量の比較. ETV耐性を有する症例でHBV DNA低下量が乏しい傾向（12週 $p=0.032$, 48週 $p=0.241$）を示した.

ADV耐性で2.1log, LAM耐性＋ETV耐性で1.0 log, 3剤耐性で0.7logであった. ETV耐性を有する6例と有さない12例の投与12週, 48週のHBV DNA減衰量を比較すると, ETV耐性を有する例で減衰量が低下した（ETV耐性なし vs ETV耐性あり 12週 1.1log vs 0.6log, $p=0.032$, 48週 1.5log vs 1.0log, $p=0.241$）（Figure 2）.

ベースラインでHBe抗原陽性を示した13例中1例が治療8週の時点で陰性となり, 1例を除くとHBe抗原量が低下した. ALTについてはベースライン, 治療後で有意な変化を認めなかった（Table 2）.

INNO-LiPA法による耐性部位の検出では, 治療48週において, 新たな耐性の出現を認めなかった. 一部の症例でコドン181のA/VがA, コドン236のTがNに変化するなどの耐性クローンの消失が認められた. ウイルス量の低下にともない1例でINNO-LiPA法による検出が不能となった（Table 3）.

本研究中に有害事象の出現による中止例は認めなかった. 2例がLAM/ADV療法の時点で腎障害のため既にADVが隔日投与となっていたが, この2例を含めてADV/ETV療法に移行後の腎障害の増悪例は認めなかった.

Table 3. ETV/ADV 療法ベースライン，48 週における耐性部位の検出

A) Baseline											
Case	Codon	80	173	180	204	181	233	236	* 184	202	250	194
	1	L	V	L	I	A	I	T	T	S	M	A
	2	L	V	L/M	I	A	I	N	T	S	M	A
	3	L	V	L/M	V	A	I	N	T/SCGA	S	M/V	A
	4	L/I	V	L/M	V/I	A	I	N	T	S	M/L	A
	5	L	V	L/M	V	A	I	N	T/ILFM	S/G	M	A
	6	L	V	L	M/I	A/T	I	N	T	S	M	A
	7	I	V	L/M	V/I	A	I	N	T	S	M	A
	8	L/I	V	L/M	M/I	A	I	N	T	S	M	A
	9	L	V	L/M	V	A	I	N	T	S/G	M	A
	10	L	V	L/M	M/V/I	A	I	N	T	S	M	A
	11	L	V	M	V	A	I	N	T	S	M	A
	12	L	V	L/M	M/V/I	A	I	N	T	S	M	A
	13	L	V/L	L/M	M/V/I	A/T	I	N	T	S	M	A
	14	L	V/L	L/M	V/I	A	I	N	T	S	M	A
	15	L/I	V	L/M	M/V/I	A	I	N	T	S	M	A
	16	L	V	L/M	M/V/I	A	I	N	T/ILFM	S/G	M	A
	17	L/I	V	L/M	M/I	A/V	I	N	T	S	M	A
	18	L	V	L/M	V	A	V	N	T/SCGA	S	M	A
B) Week 48												
Case	Codon	80	173	180	204	181	233	236	184	202	250	194
	1	L	V	L	*	A	I	N	T	S	M	A
	2	L	V	L/M	*	A	I	N	T	S	M	A
	3	L	V	M	V	A	I	N	GA/IL	S	M/I	A
	4	L/I	V	L/M	I	A	I	N	T	S	M/L	A
	5	L	V	M	V	A	I	N	T/ILFM	S/G	M	A
	6	ND	ND	ND	ND	ND	ND	ND	ND	ND	ND	ND
	7	I	V	L/M	I	A	I	N	T	S	M	A
	8	L/I	V	L/M	I	A	I	N	T	S	M	A
	9	L	V	M	V	A	I	N	T	G	M	A
	10	L	V	L/M	V	A	I	N	T	S	M	A
	11	L	V	M	V	A	*	N	T	S	M	A
	12	L	V	M	V	A	I	N	T	S	M	A
	13	L	L	M	V	A/T	I	N	T	S	M	A
	14	L	L	L/M	V	A	I	N	*	S	M	A
	15	L/I	V	L/M	V/I	A	I	N	T	S	M	A
	16	L	V	M	V	A	I	N	T/ILFM	S/G	M	A
	17	I	V	L	I	A	I	N	T	S	M	A
	18	L	V	M	V	A	V	N	SCGA	S	M	A

A：alanine，C：cysteine，G：glysine，F：phenylalanine，I：isoleucine，L：leucine，M：methionine．N：asparagine，S：serine，T：threonine，V：valine．
ND：not detected．＊：impossible to judge．

III 考 察

B型慢性肝疾患に対する核酸アナログ療法の最も重要な問題は耐性ウイルスの出現である．ETV や TDF の登場により耐性ウイルスの出現率は低下した[19]が，既に LAM 耐性を獲得してしまった多くの患者が全世界中に存在している[9]．日本肝

臓病学会ではLAM耐性例に対してはADVを併用するよう推奨している[15]．このLAM/ADV療法は多くの患者に有効であるが，一部の患者ではHBV DNAの低下量が不十分であり，HBV DNAの陰性化が得られない[16][17]．また，LAM耐性例ではLAM/ADV療法中にADV耐性が出現することが報告[20][21]されており，HBV DNAが陰性化しない，いわゆる不応例においては，新規の治療法が望まれてきた．以前われわれはLAM耐性例に対するLAM/ADV療法中にADV耐性を獲得した1例を経験したが，この症例はウイルス学的ブレイクスルーを発症し，軽度であるが肝炎の増悪をきたした．LAMを中止し，ADVは継続したままでETVを追加したところ，良好な抗ウイルス効果が得られ，ALT値も正常化した（Table 2, case 1）．この症例の経験を踏まえて，LAM/ADV療法不応例に対するADV/ETV療法の臨床研究を行った．ETVはLAM耐性とADV耐性例に[22][23]，ADVはLAM耐性とETV耐性例に対して抗ウイルス効果を発揮する[24]ことが示されており，LAM/ADV療法不応例に対するADV/ETV療法はTDFが承認されていない本邦の現状を考慮すると，また，交叉耐性を考えても理にかなった治療法と考えられる．

ADV不応例に対するETV療法の報告は近年散見されるが，いずれも症例数が少なく，短期間の成績が示されるにすぎない．40例のADV不応例（14例でADV耐性あり）に対してETVを投与した報告では，HBV DNA陰性化率が10%と低率で，6例（15%）にETV耐性の出現を認めた[25]．一方でHBe抗原陽性ADV不応14例（3例でADV耐性あり）に対するETV投与では，HBV DNA陰性化率は低いものの，15カ月の経過でHBV DNAはLAM投与歴なしで3.4log，LAM投与歴のあるもので3.9log低下し，この報告ではETV耐性の出現は認めなかった[26]．LAMとADVの2剤耐性を有する50例に対するETV投与では48週の経過でHBV DNA陰性化率は10%，HBV DNA量はベースライン6.90logより2.96logと低下した．ETV耐性はわずか1例(2%)で出現した[27]．ADV投与歴を有する症例に対するETV投与ではLAM投与歴を有する24例（9例がADV耐性あり）でHBV DNA陰性化率は42%であり，17%の症例でETV耐性が出現した[28]．報告によりウイルス陰性化率やHBV DNA低下量に差があるのは，症例数が少ないことや，人種や遺伝子型などの対象症例が異なること，過去に受けた核酸アナログの治療内容や期間に差があるためと思われる．

今回われわれが行ったLAM/ADV不応例に対するADV/ETV療法48週では平均でHBV DNAは1.2log低下した．低下量は少ないが，18例中5例が48週の治療中に2.1log未満を呈した．先に記したが，ADV不応例に対するETV単独療法によりETV耐性出現が報告されている[25][27][28]が，ADV/ETV療法では，更なる耐性の出現は認めなかった．ADVの併用投与がETV耐性を抑制した可能性が示唆された．

ADV/ETV療法中，脱落例・中止例は認めなかった．ADVによる腎障害の報告が散見される[29][30]が，ETVも腎排泄型のため注意が必要である．血清クレアチニンによる腎機能のモニターを定期的に行い，必要に応じて投与量の調節を行うことが重要である．

おわりに

LAM/ADV療法不応例に対するADV/ETV療法の成績を示した．経過観察期間が短く，少数例の検討ではあるが，HBV DNAは低下し，新たなアナログ耐性の出現は認めなかった．今後，観察期間を延長し，ADV/ETV療法の効果と安全性を検証する必要があると思われた．

文　献

1) Lavanchy D : Hepatitis B virus epidemiology, disease burden, treatment, and current and emerging prevention and control measures. J Viral Hepat 11 : 97–107 : 2004
2) Ganem D, Prince AM : Hepatitis B virus infection--natural history and clinical consequences. N Engl J Med 350 : 1118–1129 : 2004
3) Marcellin P, Lau GK, Bonino F, et al : Peginterferon alfa-2a alone, lamivudine alone, and the two in combination in patients with HBeAg-negative chronic hepatitis B. N Engl J Med 351 : 1206–

1217 : 2004
4) Janssen HI, van Zonneveld M, Senturk H, et al : Pegylated interferon alfa-2b alone or in combination with lamivudine for HBeAg-positive chronic hepatitis B : a randomised trial. Lancet 365 ; 123–129 : 2005
5) Lai CI, Chien RN, Leung NW, et al : A one-year trial of lamivudine for chronic hepatitis B. Asia Hepatitis Lamivudine Study Group. N Engl J Med 339 ; 61–68 : 1998
6) Dienstag JL, Goldin RD, Heathcote EJ, et al : Histological outcome during long-term lamivudine therapy. Gastroenterology 124 ; 105–117 : 2003
7) Liaw YF, Sung JJ, Chow WC, et al : Lamivudine for patients with chronic hepatitis B and advanced liver disease. N Engl J Med 351 ; 1521–1531 : 2004
8) Lai CL, Dienstag J, Schiff E, et al : Prevalence and clinical correlates of YMDD variants during lamivudine therapy for patients with chronic hepatitis B. Clin Infect Dis 36 ; 687–696 : 2003
9) Chang TT, Lai CL, Chien RN, et al : Four years of lamivudine treatment in Chinese patients with chronic hepatitis B. J Gastroenterol Hepatol 19 ; 1276–1282 : 2004
10) Chang TT, Gish RG, de Man R, et al : A comparison of entecavir and lamivudine for HBeAg-positive chronic hepatitis B. N Engl J Med 354 ; 1001–1010 : 2006
11) Sherman M, Yurdaydin C, Sollano J, et al : Entecavir for treatment of lamivudine-refractory, HBeAg-positive chronic hepatitis B. Gastroenterology 130 ; 2039–2049 : 2006
12) Lai CL, Shouval D, Lok AS, et al : Entecavir versus lamivudine for patients with HBeAg-negative chronic hepatitis B. N Engl J Med 354 ; 1011–1020 : 2006
13) Lok AS, McMahon BJ : Chronic hepatitis B : update 2009. Hepatology 50 ; 661–662 : 2009
14) European Association For The Study Of The Liver : EASL Clinical Practice Guidelines : management of chronic hepatitis B. J Hepatol 50 ; 227–242 : 2009
15) Kumada H, Okanoue T, Onji M, et al : Guidelines for the treatment of chronic hepatitis and cirrhosis due to hepatitis B virus infection for the fiscal year 2008 in Japan. Hepatol Res 40 ; 1–7 : 2010
16) Peters MG, Hann Hw H, Martin P, et al : Adefovir dipivoxil alone or in combination with lamivudine in patients with lamivudine-resistant chronic hepatitis B. Gastroenterology 126 ; 91–101 : 2004
17) Shakado S, Watanabe H, Tanaka T, et al : Combination therapy of lamivudine and adefovir in Japanese patients with chronic hepatitis B. Hepatol Int 2 ; 361–369 : 2008
18) Niesters HG, Zoulim F, Pichoud C, et al : Validation of the INNO-LiPA HBV DR assay (version 2) in monitoring hepatitis B virus-infected patients receiving nucleoside analog treatment. Antimicrob Agents Chemother 54 ; 1283–1289 : 2010
19) Tenny DJ, Rose RE, Baldick CJ, et al : Long-term monitoring shows hepatitis B virus resistance to entecavir in nucleoside-naïve patients is rare through 5 years of therapy. Hepatology 49 ; 1503–1514 : 2009
20) Lampertico P, Viganò M, Manenti E, et al : Low resistance to adefovir combined with lamivudine : a 3-year study of 145 lamivudine-resistant hepatitis B patients. Gastroenterology 133 ; 1445–1451 : 2007
21) Inoue J, Ueno Y, Wakui Y, et al: Four-year study of lamivudine and adefovir combination therapy in lamivudine-resistant hepatitis B patients : influence of hepatitis B virus genotype and resistance mutation pattern. J Viral Hepat 2010[Epub ahead of print]
22) Suzuki F, Toyoda J, Katano Y, et al : Efficacy and safety of entecavir in lamivudine-refractory patients with chronic hepatitis B : randomized controlled trial in Japanese patients. J Gastroentrol Hepatol 23 ; 1320–1326 : 2008
23) Kamar N, Milioto O, Alric L, et al : Entecavir therapy for adefovir-resistant hepatitis B virus infection in kidney and liver allograft recipients. Transplantation 86 ; 611–614 : 2008
24) Yatsuji H, Hiraga N, Mori N, et al : Successful treatment of an entecavir-resistant hepatitis B virus variant. J Med Virol 79 ; 1811–1817 : 2007
25) Cho SW, Koh KH, Cheong JY, et al : Low efficacy of entecavir therapy in adefovir-refractory hepatitis B patients with prior lamivudine resistance. J Viral Hepat 17 ; 171–177 : 2010
26) Reijnders JG, Pas SD, Schutten M, et al : Entecavir shows limited efficacy in HBeAg-positive hepatitis B patients with a partial virologic response to adefovir therapy. J Hepatol 50 ; 674–683 : 2009
27) Shim JH, Suh DJ, Kim KM, et al : Efficacy of entecavir in patients with chronic hepatitis B resistant to both lamivudine and adefovir or to lamivudine alone. Hepatology 50 ; 1064–1071 : 2009
28) Reijnders JG, Deterding K, Petersen J, et al : Antiviral effect of entecavir in chronic hepatitis B : influence of prior exposure to nucleos(t)ide ana-

logues. J Hepatol 52 ; 493–500 : 2010
29) Ha NB, Ha NB, Garcia RT, et al : Renal dysfunction in chronic hepatitis B patients treated with adefovir dipivoxil. Hepatology 50 ; 727–734 : 2009
30) Tamori A, Enomoto M, Kobayashi S, et al : Add-on combination therapy with adefovir dipivoxil induces renal impairment in patients with lamivudine-refractory hepatitis B virus. J Viral Hepat 17 ; 123–129 : 2010

論文受領, 平成22年9月27日
受理, 平成22年10月2日

Liver Fibrosis in Patients with Chronic Hepatitis C: Noninvasive Diagnosis by Means of Real-time Tissue Elastography—Establishment of the Method for Measurement[1]

Yohei Koizumi, MD
Masashi Hirooka, MD, PhD
Yoshiyasu Kisaka, MD, PhD
Ichiro Konishi, MD, PhD
Masanori Abe, MD, PhD
Hidehiro Murakami, MD, PhD
Bunzo Matsuura, MD, PhD
Yoichi Hiasa, MD, PhD
Morikazu Onji, MD, PhD

Purpose: To prospectively measure liver stiffness with real-time tissue elastography in patients with chronic hepatitis C and to compare the results with those of clinical assessment of fibrosis by using histologic stage as the reference standard.

Materials and Methods: All subjects gave informed consent, and the study was approved by the institutional ethics committee. Seventy hospitalized patients (46 men, 24 women; mean age, 65.5 years ± 11.7 [standard deviation]; age range, 33–87 years) with chronic hepatitis C underwent real-time elastography between January 2009 and September 2009. Elastography was performed at four liver locations by two independent observers. The elastic ratio (ratio of the value in the intrahepatic venous small vessels divided by the value in the hepatic parenchyma) was calculated and was compared with histologic fibrosis stage at liver biopsy. The elastic ratio and clinical fibrosis markers were assessed by using receiver operating characteristic (ROC) analysis. The differences between body site and observers were assessed with κ statistics and intraclass correlation coefficients (ICCs).

Results: Real-time tissue elastography cutoff values were 2.73 for F of 2 or greater, 3.25 for F of 3 or greater, and 3.93 for F of 4. No site differences were observed (κ = 0.835, ICC = 0.966), and the elastic ratio measurement was correlated between the two examiners (r^2 = 0.869, $P < .0001$). The areas under the ROC curves for elastic ratio, hyaluronic acid, type IV collagen, aspartate aminotransferase–to–platelet ratio index, FibroIndex, Forns score, and Hepascore were 0.95, 0.32, 0.73, 0.76, 0.76, 0.87, and 0.70, respectively; the elastic ratio performed better than the serum fibrosis markers and other scores.

Conclusion: Real-time tissue elastography is not invasive and could be used to evaluate liver fibrosis in patients with chronic hepatitis C.

Supplemental material: *http://radiology.rsna.org/lookup/suppl/doi:10.1148/radiol.10100319/-/DC1*

[1] From the Department of Gastroenterology and Metabology, Ehime University Graduate School of Medicine, Shitsukawa, Toon, Ehime 791-0295, Japan. Received February 9, 2010; revision requested March 24; revision received June 22; accepted July 13; final version accepted August 11. Supported by a Grant-in-Aid for Scientific Research (C) (Japan Society for the Promotion of Science, KAKENHI 21590848) and the Program for Enhancing Systematic Education in Graduate School from the Ministry of Education, Culture, Sports, Science and Technology, Tokyo, Japan. **Address correspondence to** Y.H. (e-mail: *hiasa@m.ehime-u.ac.jp*).

Chronic viral hepatitis infection increases liver fibrosis and stiffness and is an important cause of liver cirrhosis (1). Although liver biopsy is the reference standard for the diagnosis of liver fibrosis (2), it is an invasive procedure, which is difficult to perform in patients who need to be examined repeatedly to monitor the progression of liver fibrosis. Moreover, the evaluation of fibrosis with liver biopsy is associated with adverse events (3), sampling errors (4,5), and interpathologist and intrapathologist variabilities (6). Therefore, many studies have evaluated other noninvasive methods, such as the use of sonographic transient elastography (FibroScan; EchoSens, London, England) (7) and acoustic radiation force impulse (8) and laboratory tests, such as the aspartate aminotransferase-to-platelet ratio index, the FibroIndex, the Forns score, and the Hepascore, for the assessment of liver fibrosis stage.

Transient elastography is one of the techniques that can be used to evaluate mean tissue stiffness noninvasively (7). Results of several recent studies (9) have shown that measurements of liver stiffness with transient elastography are well correlated with fibrosis METAVIR stages. In addition, transient elastography is advantageous in that it can be repeatedly performed, does not require a highly experienced operator, and has a low risk of complications. However, there is a problem with reproducibility at identical measurement positions (10). In addition, it is not a real-time technique, because the image is not visible while the measurement is being taken. The reproducibility of transient elastography is also substantially reduced in patients with steatosis and increased body mass index (BMI) because the modality of ultrasonography (US) itself has limitations for visualizing the liver clearly in such patients (11).

Real-time tissue elastography is a relatively new method for the measurement of tissue elasticity. It uses a B-mode US machine, incorporating elastography into the conventional US scanner (12). In the previously reported technique, a US probe is used to slightly compress or relax the body (13), and the echo signals are captured in real time. This device calculates the relative hardness of tissue and displays this information as real-time color images (14); it can display tissue elasticity images and conventional B-mode images at the same time.

The purpose of this prospective study was to measure liver stiffness with real-time elastography in patients with chronic hepatitis C and to compare the results with those of other clinical assessments of fibrosis by using the histologic stage of fibrosis as the reference standard.

Advances in Knowledge

- In patients with hepatitis C, the areas under the receiver operating characteristic curves for prediction of fibrosis by means of elastic ratio, hyaluronic acid level, type IV collagen level, aspartate aminotransferase-to-platelet ratio index, FibroIndex, Forns score, and Hepascore were 0.95, 0.32, 0.73, 0.76, 0.76, 0.87, and 0.70, respectively, indicating that the elastic ratio performed better than the other serum fibrosis markers and scores.
- For METAVIR stages identified at histologic examination, real-time elastography cutoff values were 2.73 for F of 2 or greater, 3.25 for F of 3 or greater, and 3.93 for F of 4.
- Our results were independent of observer ($r^2 = 0.869$, $P < .0001$) and measurement positioning site (intraclass correlation coefficient: 0.966, $\kappa = 0.835$).

Implications for Patient Care

- Real-time elastography is not invasive and could be used to repeatedly evaluate liver fibrosis.
- Real-time elastography could be a powerful tool for time-course evaluation of liver cirrhosis during antiviral therapy.

Materials and Methods

Patients

The study protocol was approved by the institutional review board, and written informed consent was obtained. All enrolled patients underwent liver biopsy as part of the study. Seventy patients with chronic hepatitis C (mean age, 65.5 years ± 11.7 [standard deviation]; range, 33–87 years) were hospitalized in the Department of Gastroenterology and Metabology, Ehime University Hospital, Japan, from January 2009 to September 2009, and liver stiffness, which is related to the grade of liver fibrosis, was measured. Of the 70 patients, 46 were men (mean age, 63.5 years ± 13.9; range, 33–87 years), and 24 were women (mean age, 66.6 years ± 10.3; range, 46–84 years).

Inclusion criteria were the presence of hepatitis C virus (HCV) ribonucleic acid in serum according to real-time polymerase chain reaction and positive HCV antibody. The exclusion criteria were ascites (because that might interfere with measurements), coinfection with other viruses such as hepatitis B virus, other liver diseases such as primary biliary

Published online
10.1148/radiol.10100319

Radiology 2011; 258:610–617

Abbreviations:
AUC = area under the ROC curve
BMI = body mass index
CI = confidence interval
ICC = intraclass correlation coefficient
ROC = receiver operating characteristic
ROI = region of interest

Author contributions:
Guarantors of integrity of entire study, Y. Koizumi, M.H., Y. Kisaka, I.K., M.A., B.M., Y.H., M.O.; study concepts/study design or data acquisition or data analysis/interpretation, all authors; manuscript drafting or manuscript revision for important intellectual content, all authors; manuscript final version approval, all authors; literature research, Y. Koizumi, M.H., Y. Kisaka, I.K., M.A., B.M., Y.H.; clinical studies, Y. Koizumi, M.H., Y. Kisaka, I.K., M.A., H.M., B.M., Y.H.; experimental studies, Y. Koizumi, M.H., Y. Kisaka, I.K., M.A., Y.H.; statistical analysis, Y. Koizumi, M.H., Y. Kisaka, I.K., M.A., Y.H.; and manuscript editing, Y. Koizumi, M.H., Y. Kisaka, I.K., M.A., B.M., Y.H., M.O.

Authors stated no financial relationship to disclose.

Figure 1

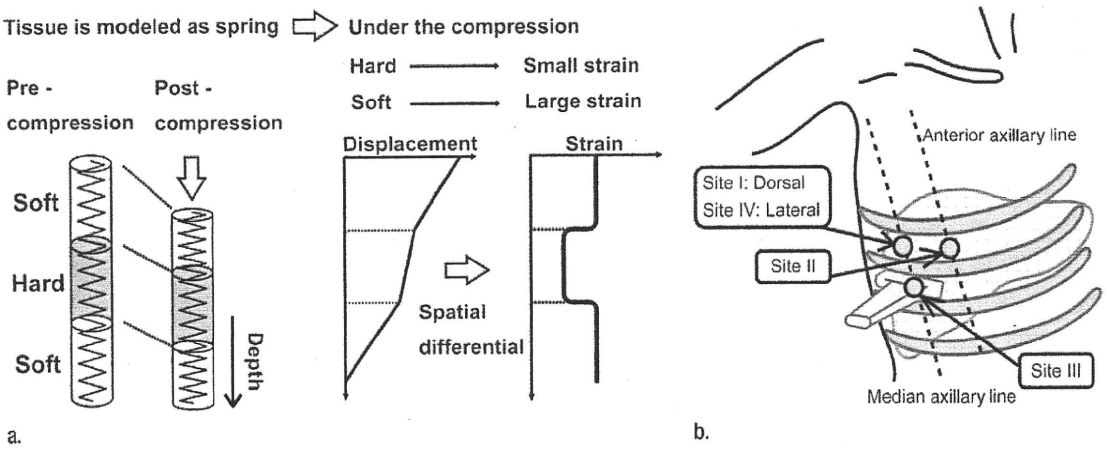

Figure 1: **(a)** The underlying method of real-time tissue elastography is the measurement and imaging of the strain distribution by adding the static pressure from the body surface; this is illustrated as a spring model. **(b)** The four measurement sites for real-time tissue elastography.

cirrhosis, and excessive alcohol consumption. (So that we could compare the METAVIR stages, which grade liver fibrosis only in patients with hepatitis C).

BMI and skin fold thickness were measured to determine whether they had any effects on real-time tissue elastography measurements.

Method for Measurement of Liver Stiffness

The underlining principle of real-time tissue elastography is illustrated in Figure 1a by using a spring model. When a spring is compressed, displacement in each section of the spring depends on the stiffness of the spring: A soft spring compresses more than a hard spring. The strain distribution, and in turn the stiffness in the spring, is measured by spatially differentiating the displacement at each location. On the basis of a previous report (13), we believed that compressing and relaxing the tissue with the US probe would be needed to measure the stiffness. However, we determined that we could measure the liver stiffness without adding any pressure from the probe because the liver itself receives pressure from the heartbeat automatically. Reflected US echoes are then used to compute the displacement and, thus, the strain distribution in the tissue. The examiners measured liver stiffness at four sites (Fig 1b), using the same positioning sites of the body as Boursier et al (10). The measurement sites were defined as follows: Site I was the dorsal decubitus and on the median axillary line and the first intercostal space; site II, the dorsal decubitus and on the anterior axillary line and the first intercostal space; site III, the dorsal decubitus and on the median axillary line and the second intercostal space; and site IV, the lateral decubitus and on the median axillary line and the first intercostal space. Real-time tissue elastography was performed five times at four measurement sites by two observers for each patient, in exhalation or inspiration to ensure that the liver was adequately depicted. The mean of the five measurements was calculated for comparison with histologic results.

Elastic Ratio

Hepatic elasticity was measured by using a US scanner with real-time tissue elastography (EUB-7500; Hitachi Medical Systems, Tokyo, Japan). We used a linear probe (EUP-L52; central frequency, 5.5 MHz). This scanner displays the color-coded elastography image overlaid on the B-mode image in real time (Fig 2a). Because this displayed color-coded elastography image shows only the relative tissue stiffness, a quantitative measuring technique called the elastic ratio was utilized.

The elastic ratio is the ratio of strain distribution in two selected regions of interest (ROIs). First, it was important to identify whether the hepatic vein or the portal vein would be a better internal control. We measured the value in the hepatic vein and portal vein for all 70 enrolled patients. The ROC curves of the elastic ratio calculated by using the ROI of the hepatic vein and the ROI of the portal vein as internal controls are shown in Figure 2b. The areas under the ROC curves (AUCs) of the elastic ratios obtained by using the hepatic vein as an internal control were higher than those obtained by using the portal vein as an internal control (intraclass correlation coefficient [ICC]: 0.953 [95% confidence interval {CI}: 0.903, 0.998] vs 0.731 [95% CI: 0.649, 0.886]; $P = .0006$). On the basis of the AUCs, the hepatic veins were used as an internal control. The ROI was placed on intrahepatic venous small vessels with a diameter of less than 3 mm and the hepatic parenchyma simultaneously. Subsequently, the ratio of the value in the intrahepatic venous small vessels was divided by the value in the hepatic parenchyma to generate the elastic ratio.

The elasticity of the hepatic vein was used as the reference because the elasticity of the veins does not change over time, since they do not undergo

Figure 2

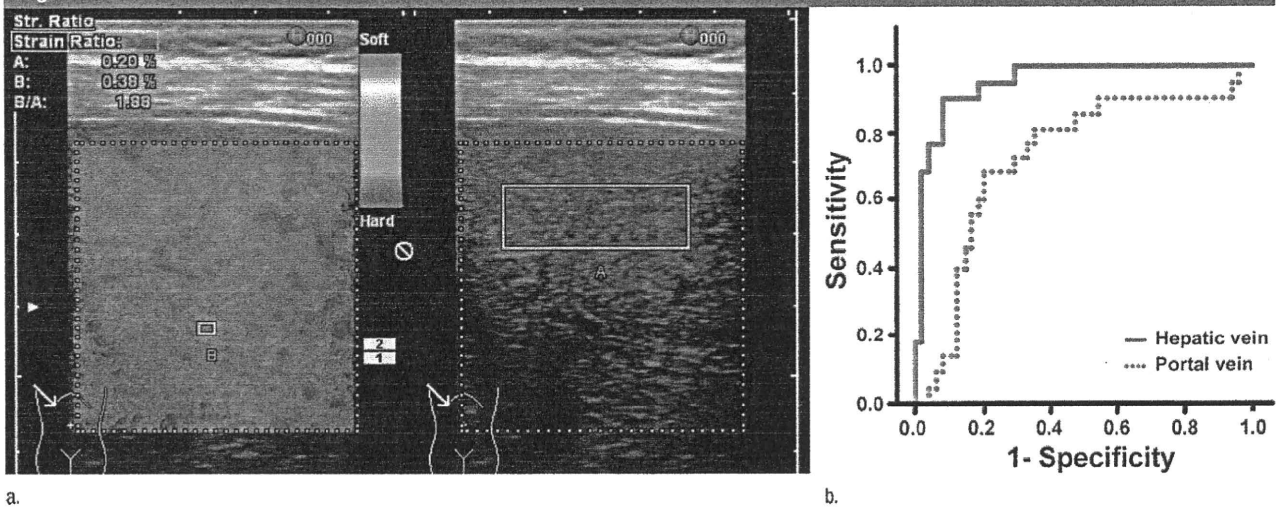

Figure 2: **(a)** The elastic ratio is measured between the tissue compressibility of the liver (right) and that of the intrahepatic small vessel (left). Red indicates that tissue is soft, and blue indicates that it is hard. Information about displacement becomes the basis of the elastic information and is obtained by using a supersonic wave signal. **(b)** Receiver operating characteristic (ROC) curves of the elastic ratio obtained by using the hepatic vein or portal vein as an internal control.

transformations with disease, such as arteriosclerosis, and it also does not increase or decrease even when liver parenchyma becomes stiffer. Thus, small vessels with a diameter of 3 mm in the liver were used as the standard for computing the elasticity ratio, and the ROI was set as large as possible (usually 0.3 × 0.5 cm). The ROI in the liver parenchyma was placed 1 cm from the liver surface and was 2 × 1 cm in size. A higher elastic ratio indicates harder hepatic elasticity, corresponding to a higher stage of fibrosis. None of the patients had liver tumors in the measurement site that might have interfered with the real-time tissue elastography.

Observers

Two hepatologists (M.H. and Y. Koizumi, with 13 and 6 years of experience, respectively) performed the liver stiffness evaluation with real-time tissue elastography; each had already performed at least 100 liver stiffness evaluations (M.H., 350; Y. Koizumi, 120) prior to the beginning of the study. Each observer measured the elastic ratio five times at four sites (Fig 1b). The second observer was blinded to the results of the first observer. Measurement time for each measurement site (time from the beginning of measurement until completion to identify the elastic ratio with five measurements after placing the ROI) was recorded for each observer. For measurement site IV, the measurement time included the time for movement of the patient.

Liver Histologic Assessment

US-guided percutaneous liver biopsy (1.6-mm-diameter and 150-mm-long needle, suction technique) was performed within 1 week after hospitalization. Liver biopsy samples less than 12 mm long were excluded, because a sampling error for identifying liver fibrosis may occur with such samples (4). Liver biopsy samples were fixed in formalin and embedded in paraffin. Slices (4 μm thick) were stained with hematoxylin-eosin and impregnated with silver. Liver biopsies that contained fewer than five portal tracts (except for cirrhosis) were excluded from the histologic analysis. Fibrosis was staged by two pathologists (one of whom was I.K., with 16 years of experience), who were blinded to all patient characteristics. Fibrosis was staged on a four-point scale according to METAVIR (F0 indicated no fibrosis; F1, portal fibrosis without septa; F2, portal fibrosis and few septa; F3, numerous septa without cirrhosis; F4, cirrhosis) (15). Activity was graded according to METAVIR as A0, none; A1, mild; A2, moderate; and A3, severe (16). Lipid share was defined as mild, 0%–30%; moderate, 30%–60%; and severe, more than 60%.

Serum Fibrosis Markers

Levels of the following blood parameters were determined: aspartate aminotransferase, alanine aminotransferase, total bilirubin, platelets, gamma-glutamyl transferase, cholesterol, urea, hyaluronic acid, type IV collagen, cholinesterase, α1 and α2 globulins, β globulins, γ-globulins, prothrombin index, apolipoprotein-A1, haptoglobin, and ferritin. The aspartate aminotransferase (AST)–to–platelet ratio index (17) was calculated as follows: (AST/UNL · 100)/platelet count. (UNL is the upper limit of the normal aspartate aminotransferase.) The FibroIndex (18) was calculated as 1.738 − 0.064 (platelet count) + 0.005 (AST) + 0.463 (gamma-globulin). Forns score (19) was calculated as 7.811 − 3.131 ln(platelet count) + 0.781 ln(gamma-glutamyl transferase) + 3.467 ln(age) − 0.014 (cholesterol). Hepascore (20) was calculated as $y/(1 + y)$, $y = \exp[-4.185818 - (0.0249 \cdot \text{age}) + 0.7464 \cdot \text{sex}] + (1.0039 \cdot \alpha2\text{-macroglobulin}) + (0.0302 \cdot \text{hyaluronic acid}) + (0.0691 \cdot \text{bilirubin}) - (0.0012 \cdot \text{gamma-glutamyl transferase})$.

Statistical Analysis

The AUC of the elastic ratio was then compared with that derived from standard laboratory tests published in the literature, including the aspartate aminotransferase-to-platelet ratio index, FibroIndex, Forns score, and Hepascore (17–20). The ROC curve was prepared by using a statistical software package (JMP, version 8; SAS Institute Japan, Tokyo, Japan).

The diagnostic performance of liver stiffness evaluation and fibrosis was determined in terms of sensitivity, specificity, positive predictive value, negative predictive value, diagnostic accuracy, and AUC. The optimal cutoff values for liver stiffness were chosen to maximize the sum of sensitivity and specificity, and positive and negative predictive values were computed for those cutoff values.

Stiffness measurements were not normally distributed. Therefore, the elastic ratio was compared with the categories of the consensus fibrosis stage by using the Kruskal-Wallis nonparametric analysis of variance test. Correlations between the elastic ratio and the histologic fibrosis stage were also analyzed by using Spearman correlation coefficients.

The correlations between the values of each observer's real-time tissue elastography measurements, as well as the site differences, were evaluated by calculating κ coefficients and ICCs. The κ coefficient was defined as follows: poor, $\kappa < 0.4$; fair to good, $0.4 \leq \kappa < 0.75$; and excellent, $0.75 \leq \kappa$ (21). The ICC was defined as follows: slight, $0 \leq ICC < 0.20$; fair, $0.21 \leq ICC < 0.40$; moderate, $0.41 \leq ICC < 0.60$; substantial, $0.61 \leq ICC < 0.80$; and almost perfect, $ICC > 0.81$ (22).

The estimated sample sizes according to the two-sample Student *t* test in the F1–F3 group and F4 groups were 20 and 20 respectively, given a type I error of .05, a type II error of .2, and an effect size of 1.785. Multivariate stepwise logistic regression models were used to identify independent significant factors among serum fibrosis markers, METAVIR fibrosis stage, and activity grade, steatosis, BMI, and skin fold thickness for the elastic ratio determined with real-time tissue elastography. The statistical analyses were performed by using the JMP statistical software.

Table 1

Patient Characteristics

Characteristic*	All Patients (*n* = 70)	Men (*n* = 46)	Women (*n* = 24)
Age (y)	65.5 ± 11.7	66.6 ± 10.3	63.4 ± 13.9
BMI (kg/m²)	23.2 ± 3.37	22.8 ± 3.05	23.9 ± 3.82
ALT level (IU/L)	42.8 ± 31.4	46.3 ± 35.0	35.9 ± 21.9
Serum albumin level (g/dL)	3.68 ± 0.60	3.61 ± 0.61	3.81 ± 0.57
Platelet count ($10^4/\mu L$)	14.1 ± 7.12	14.1 ± 7.68	14.1 ± 6.05
Prothrombin time (%)	91.6 ± 18.1	89.3 ± 17.7	95.9 ± 18.4
Total bilirubin (mg/dL)	0.9 ± 0.44	0.95 ± 0.49	0.77 ± 0.30
GGT level (IU/L)	55.5 ± 46.8	62.6 ± 48.1	41.9 ± 41.6
Child-Pugh class			
A	63	40	23
B	7	6	1
C	0	0	0
Histologic fibrosis stage			
F1	12	6	6
F2	16	10	6
F3	19	12	7
F4	23	18	5
Histologic activity grade			
A0	1	1	0
A1	67	44	23
A2	2	1	1
A3	0	0	0
Histologic steatosis			
Mild	68	46	22
Moderate	2	0	2
Severe	0	0	0

Note.—Data are means ± standard deviations or numbers of patients.

* ALT = alanine aminotransferase, GGT = gamma-glutamyl transferase.

Results

Patients

Between January 2009 and September 2009, 70 patients met the inclusion criteria (Table 1). There were no significant differences in age ($P = .54$) or BMI ($P = .31$) between men and women. Gamma-glutamyl transferase was significantly higher in men ($P = .02$), but no significant difference was seen in the other biochemical tests between men and women (Table 1).

The rates of interobserver agreement in determining each fibrosis stage at each site were: site I, 81.4% (57 of 70 patients); site II, 71.4% (50 of 70 patients); site III, 74.3% (52 of 70 patients); and site IV, 75.7% (53 of 70 patients). For F4 or non-F4, the rate of interobserver agreement was: site I, 97.1% (68 of 70 patients); site II, 88.6% (62 of 70 patients); site III, 88.6% (62 of 70 patients); and site IV, 92.9% (65 of 70 patients). The mean κ value for F4 or non-F4 according to the elastic ratio was excellent at each site (site I, $\kappa = 0.94 \pm 0.04$ [standard error of the mean]; site II, $\kappa = 0.77 \pm 0.075$; site III, $\kappa = 0.77 \pm 0.08$; and site IV, $\kappa = 0.85 \pm 0.06$) (Table 2). At sites I–IV, the κ value, ICCs and 95% CIs indicated that the interobserver agreement was almost the same. The time for measurement was within 5 minutes for each measurement site, and the total measurement time for four sites was not significantly different between the two examiners ($P = .93$).

Table 2

Influence of Measurement Site on Interobserver Agreement

Parameter	Measurement Site				
	I	II	III	IV	All
ICC	0.95	0.92	0.91	0.94	0.97
95% CI	0.92, 0.97	0.87, 0.95	0.83, 0.93	0.90, 0.96	0.95, 0.98
Diagnosis of F1–F4 fibrosis (κ)	0.73	0.60	0.57	0.66	0.64
Diagnosis of F4 or non-F4 fibrosis (κ)	0.94	0.77	0.77	0.86	0.84
Measurement time for M.H. (min)	2.78 ± 1.38	2.92 ± 1.31	2.78 ± 1.38	3.12 ± 1.47	11.7 ± 1.66
Measurement time for Y. Koizumi (min)	2.82 ± 1.41	2.95 ± 1.29	2.77 ± 1.35	3.23 ± 1.41	11.9 ± 1.83

Figure 3

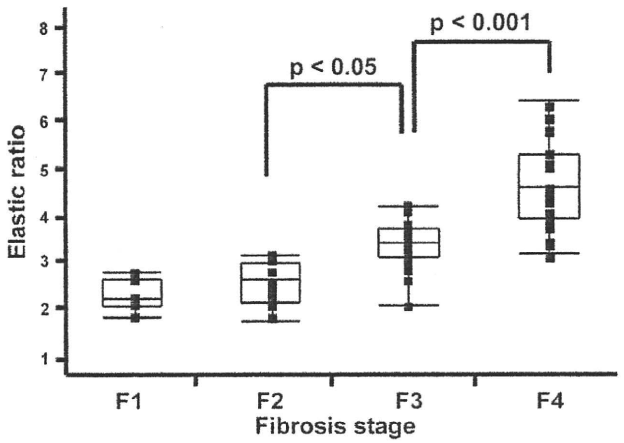

Figure 3: Graph shows elastic ratio for each fibrosis stage. The vertical axis is logarithmic scale. Tops and bottoms of the boxes = 1st and 3rd quartiles. The length of the box thus represents the interquartile range within which 50% of the values are located.

Figure 4

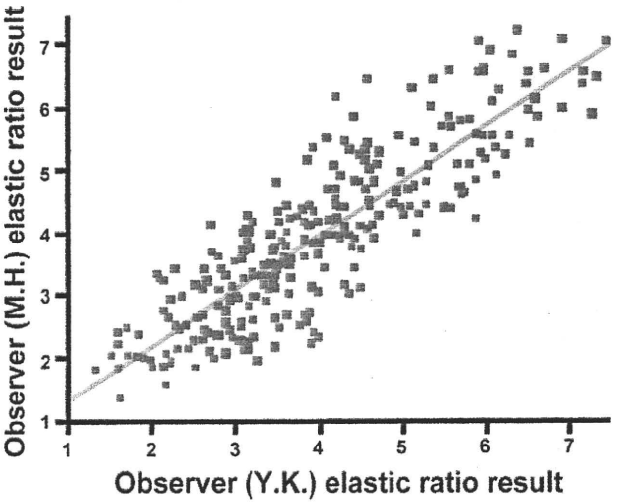

Figure 4: Graph shows correlation of elastic ratio measurement results between two examiners (Y. Koizumi and M.H., $r^2 = 0.869$, $P < .0001$).

Relationship between Liver Elastic Ratio and Histologic Parameters

The median value (95% CI) of the liver elastic ratio compared with the METAVIR fibrosis stage is shown in Figure 3: F1, 2.21 (1.94, 2.70); F2, 2.69 (2.29, 2.97); F3, 3.42 (3.07, 3.65); and F4, 4.66 (4.40, 4.93). The elastic ratios of each METAVIR fibrosis stage at liver biopsy differed significantly from each other (F2 vs F3, $r^2 = 0.36$, $P = .02$; F3 vs F4, $r^2 = 0.41$, $P < .001$). We found a significant correlation between fibrosis stage and the elastic ratio ($\rho = 0.82$, $P < .001$). However, there was no correlation between the METAVIR activity grade and the elastic ratio ($P = .36$). The elastic ratios identified by the two examiners were strongly correlated (Fig 4) and did not differ significantly. The optimal elastic ratio cutoff values obtained for the entire population, as well as the corresponding sensitivities and specificities, are shown in Table 3. The apparent cutoff values for F ≥ 2 (2.79) and F ≥ 3 (3.25) were close, but F ≥ 3 had higher sensitivity and specificity (85.4% and 96.4%) than F ≥ 2 (82.8% and 90.9%); however, the differences were not significant (sensitivity, $P = .67$; specificity, $P = .10$). A clear cutoff value (3.93) was obtained for F = 4, with sensitivity and specificity of 90.9% and 91.5%, respectively.

Mean real-time tissue elastography liver parenchyma values were as follows: site I, 0.07 ± 0.05 (standard deviation); site II, 0.08 ± 0.045; site III, 0.08 ± 0.06; site IV, 0.09 ± 0.05; and total, 0.08 ± 0.05 ($P = .09$). The mean absolute value of the hepatic vein vessels on real-time tissue elastography did not differ significantly according to site (site I, 0.25 ± 0.14; site II, 0.25 ± 0.12; site III, 0.26 ± 0.19; site IV, 0.25 ± 0.12; and total, 0.25 ± 0.13, $P = .94$).

Relationship between Liver Elastic Ratio and Fibrosis Blood Tests

The AUCs for diagnosis of fibrosis with elastic ratio, hyaluronic acid, type IV collagen (Fig 5a), aspartate aminotransferase-to-platelet ratio index, FibroIndex, Forns score, and Hepascore (Fig 5b) were 0.95, 0.32, 0.73, 0.76, 0.76, 0.87, and 0.70, respectively (Table 4). In the multivariate stepwise regression analysis, METAVIR fibrosis stage ($P < .0001$) and prothrombin time ($P = .0013$) were

Table 3

Elastic Ratio for Determination of METAVIR F Stage

Parameter	F ≥ 2 (F1 vs F2–F4)	F ≥ 3 (F1–F2 vs F3–F4)	F = 4 (F1–F3 vs F4)
AUC	0.89	0.94	0.95
Optimal cutoff	2.73	3.25	3.93
Sensitivity (%)	82.8	85.4	90.9
Specificity (%)	90.9	96.4	91.5
Positive predictive value (%)	98.0	97.2	83.3
Negative predictive value (%)	50.0	81.8	95.6

Table 4

Results of Comparison between Real-time Elastography and Fibrosis Blood Tests

Parameter	Real-Time Elastography	APRI*	Forns Score	FibroIndex	Hepascore
AUC	0.95	0.76	0.87	0.76	0.70
Sensitivity (%)	90.9	81.8	68.2	63.6	63.4
Specificity (%)	91.5	74.4	95.8	87.5	70.8

* APRI = aspartate aminotransferase–to–platelet ratio index.

Figure 5

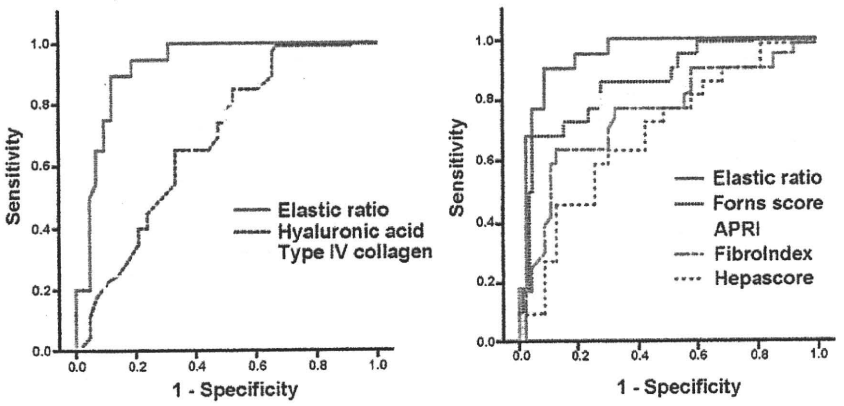

Figure 5: **(a, b)** ROC curves for diagnosis of liver fibrosis (F4) with real-time elastography. The AUC for the diagnosis of clinically important liver fibrosis or cirrhosis (F4) by using the EUB-7500 (Hitachi Medical Systems) device is superior to the results with **(a)** blood parameters or **(b)** calculated fibrosis indexes. *APRI* = aspartate aminotransferase–to–platelet ratio index.

independently associated with the elastic ratio.

Skin Fold Thickness and BMI

Interobserver agreement for elastic ratio was excellent when the skin fold thickness was less than 20 mm and BMI was less than 25 kg/m^2. However, for patients with a skin fold thickness greater than 20 mm or a BMI greater than 25 kg/m^2, the interobserver agreement was not as good (Table 5).

Discussion

There are many reports and approaches to evaluating liver stiffness without liver biopsy. Among them, the FibroScan appears useful (23,24), but there are few reports about its reproducibility. Boursier et al (10) reported that the reproducibility of the liver hardness measurement obtained by using the FibroScan differs according to measurement position. Since the absolute value of liver stiffness at real-time tissue elastography was variable, we established a procedure to obtain reproducibility by using the signal of the small hepatic veins as a reference. Using the elastic ratio, we found no difference in reproducibility for four measurement positions. Moreover, real-time tissue elastography has other advantages compared with the FibroScan or the acoustic radiation force impulse (Appendix E1 [online]).

We checked the reproducibility of the elastic ratio derived from real-time tissue elastography. The real-time tissue elastography procedure reported previously (13) involves applying pressure in the intercostal space with a probe; thus, when the pressure applied with the probe differs, the real-time tissue elastography value changes. This means that the value of liver stiffness differs not only with each observer, but also within the same observer. Therefore, we put a probe in the intercostal space and conducted the examination with no added pressure, because when observers add pressure during measurement, observer bias may occur. The liver itself receives pressure from the heartbeat automatically, so the elastic ratio could be measured without adding any pressure with the probe. Thus, observer variability can be lessened with this procedure.

Fatty change of the liver affects the evaluation of liver stiffness with the FibroScan (11). We performed a multivariate stepwise regression analysis to identify factors that affect real-time tissue elastography. Skin fold thickness, BMI, and liver steatosis were not identified as factors affecting the elastic ratio determined by using real-time tissue elastography, while fibrosis stage was a factor. Therefore, real-time tissue elastography may measure the degree of fibrosis. Only for patients with a skin fold thickness greater than 20 mm or BMI greater than 25 kg/m^2 did the interobserver agreement have a wider range, though the difference was not significant (perhaps owing to the small

Table 5

Results according to BMI and Skin Fold Thickness

Parameter	Group 1	Group 2	Group 3	Group 4	Group 5
BMI (kg/m^2)	<19 (n = 5)	≥19 To <22 (n = 21)	≥22 To <25 (n = 27)	≥25 To <28 (n = 9)	≥28 (n = 8)
ICC	0.91	0.94	0.90	0.88	0.88
95% CI	−0.39, 1.0	0.81, 0.98	0.77, 0.96	0.36, 0.94	0.39, 0.98
Skin fold thickness (mm)	<15 (n = 15)	≥15 To <20 (n = 37)	≥20 To <25 (n = 13)	≥25 (n = 5)	...
ICC	0.95	0.92	0.83	0.81	...
95% CI	0.83, 0.98	0.84, 0.96	0.51, 0.95	−0.68, 1.00	...

sample size). The elastic ratio could be calculated for the two patients with BMIs greater than 30 kg/m^2. Further studies involving more severely obese individuals will be needed to confirm the usefulness of real-time tissue elastography for such patients.

The elastic ratio obtained by using real-time tissue elastography performed better than serum fibrosis markers and scores of fibrotic change based on blood laboratory tests. However, our study still had limitations. It is difficult to evaluate certain types of patients with B mode US, including those with thick, fat tissue under the skin; a history of abdominal operations; difficulty stopping breathing; too much liver atrophy; or a large amount of ascites. We had only two observers, each with experience with the modality, and used only one US machine. Therefore, our results might not be applicable to other individuals with less experience. Our cutoffs for determination of accuracy were based on our own results and therefore are likely overestimates of performance.

In summary, in patients with chronic hepatitis C, real-time tissue elastography allows for noninvasive assessment of fibrosis that does not vary with the sites we tested or by observer and performs better than fibrosis indexes calculated by using blood laboratory tests.

Acknowledgments: The authors thank Ravi Managuli, PhD, RDMS (Department of Bioengineering, University of Washington, Seattle, Wash), for assistance in editing the technical comments and Yoshiko Soga, MD, PhD (Pathology Division, Ehime University Hospital, Ehime, Japan), for evaluating the histologic features of liver specimens.

References

1. Lauer GM, Walker BD. Hepatitis C virus infection. N Engl J Med 2001;345(1):41–52.
2. Strader DB, Wright T, Thomas DL, Seeff LB; American Association for the Study of Liver Diseases. Diagnosis, management, and treatment of hepatitis C. Hepatology 2004; 39(4):1147–1171. [Published correction appears in Hepatology 2004;40(1):269.]
3. Cadranel JF, Rufat P, Degos F. Practices of liver biopsy in France: results of a prospective nationwide survey. For the Group of Epidemiology of the French Association for the Study of the Liver (AFEF). Hepatology 2000;32(3):477–481.
4. Pagliaro L, Rinaldi F, Craxì A, et al. Percutaneous blind biopsy versus laparoscopy with guided biopsy in diagnosis of cirrhosis: a prospective, randomized trial. Dig Dis Sci 1983;28(1):39–43.
5. Regev A, Berho M, Jeffers LJ, et al. Sampling error and intraobserver variation in liver biopsy in patients with chronic HCV infection. Am J Gastroenterol 2002;97(10):2614–2618.
6. Rousselet MC, Michalak S, Dupré F, et al. Sources of variability in histological scoring of chronic viral hepatitis. Hepatology 2005;41(2):257–264.
7. Sandrin L, Fourquet B, Hasquenoph JM, et al. Transient elastography: a new noninvasive method for assessment of hepatic fibrosis. Ultrasound Med Biol 2003;29(12): 1705–1713.
8. Friedrich-Rust M, Ong MF, Martens S, et al. Performance of transient elastography for the staging of liver fibrosis: a meta-analysis. Gastroenterology 2008;134(4):960–974.
9. Friedrich-Rust M, Wunder K, Kriener S, et al. Liver fibrosis in viral hepatitis: noninvasive assessment with acoustic radiation force impulse imaging versus transient elastography. Radiology 2009;252(2):595–604.
10. Boursier J, Konaté A, Gorea G, et al. Reproducibility of liver stiffness measurement by ultrasonographic elastometry. Clin Gastroenterol Hepatol 2008;6(11):1263–1269.
11. Fraquelli M, Rigamonti C, Casazza G, et al. Reproducibility of transient elastography in the evaluation of liver fibrosis in patients with chronic liver disease. Gut 2007;56(7): 968–973.
12. Yamakawa M, Nitta N, Shiina T, et al. High-speed freehand tissue elasticity imaging for breast diagnosis. Jpn J Appl Phys 2003;42: 3265–3270.
13. Friedrich-Rust M, Ong MF, Herrmann E, et al. Real-time elastography for noninvasive assessment of liver fibrosis in chronic viral hepatitis. AJR Am J Roentgenol 2007; 188(3):758–764.
14. Shiina T. Real time tissue elasticity imaging using the combined autocorrelation method. J Med Ultrason 1999;26(2):57–66.
15. Intraobserver and interobserver variations in liver biopsy interpretation in patients with chronic hepatitis C. The French METAVIR Cooperative Study Group. Hepatology 1994; 20(1 pt 1):15–20.
16. Bedossa P, Poynard T. An algorithm for the grading of activity in chronic hepatitis C. The METAVIR Cooperative Study Group. Hepatology 1996;24(2):289–293.
17. Wai CT, Greenson JK, Fontana RJ, et al. A simple noninvasive index can predict both significant fibrosis and cirrhosis in patients with chronic hepatitis C. Hepatology 2003;38(2):518–526.
18. Koda M, Matunaga Y, Kawakami M, Kishimoto Y, Suou T, Murawaki Y. FibroIndex, a practical index for predicting significant fibrosis in patients with chronic hepatitis C. Hepatology 2007;45(2):297–306.
19. Forns X, Ampurdanès S, Llovet JM, et al. Identification of chronic hepatitis C patients without hepatic fibrosis by a simple predictive model. Hepatology 2002;36(4 pt 1): 986–992.
20. Adams LA, Bulsara M, Rossi E, et al. Hepascore: an accurate validated predictor of liver fibrosis in chronic hepatitis C infection. Clin Chem 2005;51(10):1867–1873.
21. Fleiss JL. Statistical methods for rates and proportions. 2nd ed. New York, NY: Wiley, 1981:218.
22. Landis JR, Koch GG. The measurement of observer agreement for categorical data. Biometrics 1977;33(1):159–174.
23. Harada N, Soejima Y, Taketomi A, et al. Assessment of graft fibrosis by transient elastography in patients with recurrent hepatitis C after living donor liver transplantation. Transplantation 2008;85(1):69–74.
24. Fraquelli M, Rigamonti C. Diagnosis of cirrhosis by transient elastography: what is hidden behind misleading results. Hepatology 2007;46(1):282; author reply 282–283.

Regulatory Peptides 166 (2011) 28–35

Contents lists available at ScienceDirect

Regulatory Peptides

journal homepage: www.elsevier.com/locate/regpep

Mutational analysis of predicted extracellular domains of human growth hormone secretagogue receptor 1a

Teruhisa Ueda, Bunzo Matsuura *, Teruki Miyake, Shinya Furukawa, Masanori Abe, Yoichi Hiasa, Morikazu Onji

Department of Gastroenterology and Metabology, Ehime University Graduate School of Medicine, Toon, Ehime 791-0295, Japan

ARTICLE INFO

Article history:
Received 15 March 2010
Received in revised form 19 July 2010
Accepted 11 August 2010
Available online 18 August 2010

Keywords:
Growth hormone secretagogue receptor
Ghrelin
GHRP-6
Receptor mutagenesis

ABSTRACT

The Class A family of guanine nucleotide-binding protein (G protein)-coupled receptors that includes receptors for motilin, ghrelin, and growth hormone secretagogue (GHS) has substantial potential importance as drug targets. Understanding of the molecular basis of hormone binding and receptor activation should provide insights helpful in the development of such drugs. We previously reported that Cys residues and the perimembranous residues in the extracellular loops and amino-terminal tail of the motilin receptor are critical for peptide ligand, motilin, binding and biological activity. In the current work, we focused on the predicted extracellular domains of the human GHS receptor 1a, and identified functionally important residues by using sequential deletions ranging from one to twelve amino acid residues and site-directed replacement mutagenesis approach. Each construct was transiently expressed in COS cells, and characterized for ghrelin- and growth hormone releasing peptide (GHRP)-6-stimulated intracellular calcium responses and ghrelin radioligand binding. Cys residues in positions 116 and 198 in the first and second extracellular loops and the perimembranous Glu^{187} residue in the second extracellular loop were critical for ghrelin and GHRP-6 biological activity. These results suggest that Cys residues in the extracellular domains in this family of Class A G protein-coupled receptor is likely involved in the highly conserved and functionally important disulfide bond, and that the perimembranous residues contribute peptide ligand binding and signaling.

1. Introduction

Human ghrelin, a 28-amino acid peptide with an n-octanoylation of the Ser residue in its third position, is secreted by endocrine cells of the stomach, termed X/A-like or ghrelin cells, and particularly found in the gastric fundus [1,2]. Ghrelin is the only known circulating orexigenic hormone acting at hypothalamus. Ghrelin also acts at pituitary to powerfully stimulate growth hormone secretion [1,3,4]. Biological actions of exogenous ghrelin have been documented, including its effects on gut motility, pancreatic exocrine secretion, glucose homeostasis, cardiovascular function, immunity, and inflammation [1,5–10].

In general, if a new hormone is discovered, then its receptor is detected and the development of its derivative is started. However, ghrelin and its receptor, growth hormone secretagogue (GHS) receptor, follow the reverse pattern. In the 1970 s, derivatives of growth hormone-releasing peptide (GHRP) were found. In particular, GHRP-6 (developed in 1984) and GHRP-2 (developed in 1992) more strongly promote the release of growth hormone than endogenous growth hormone-releasing hormone (GHRH). Natural peptide, GHRH, and its receptors were detected in patients suffering from acromegaly, but GHRP cannot affect the GHRH receptor directly. In 1996, GHS receptor, that belongs to the class A guanine nucleotide-binding protein (G protein)-coupled receptors and has binding capacity for GHRP, was cloned by Howard et al. [11]. The full-length human GHS receptor cDNA type 1a encodes 366 amino acids, whereas type 1b encodes a truncated version of the GHS receptor (stop codon at the end of the third intracellular loop). As a result, type 1b cDNA expressed in eukaryotic cells fail to respond to GHS addition. In 1999, ghrelin was finally identified as an endogenous ligand for GHS receptor [1].

Understanding of the molecular basis of hormone binding and activation of receptors provides important insights into the active conformation of such receptors, providing critical information helpful for the design and refinement of receptor-active drugs. Several ghrelin analogs might be useful for medical treatment of disorders such as anorexia and short stature. There have already been reports about point mutations of GHS receptor, I134T, V160M, A204E, and F279L, in patients who were unusually short stature and who experienced excessive hunger, however, phenotypes of the patients with these point mutations still remain unclear, particularly in heterozygous carriers [12–16]. Holst et al. have reported that four residues of 22 positions in the transmembrane domains of the receptor,

* Corresponding author. Shitsukawa 454, Toon, Ehime 791-0295, Japan. Tel.: +81 89 960 5308; fax: +81 89 960 5310.
E-mail address: bmatsu@m.ehime-u.ac.jp (B. Matsuura).

0167-0115/$ – see front matter © 2010 Elsevier B.V. All rights reserved.
doi:10.1016/j.regpep.2010.08.002

computationally considered binding site for ghrelin, GHPR-6, and non-peptide agonists, were functionally important. Deletion or replacement of residues in the transmembrane domains causes large changes of structure of the receptor.

There have been no previous reports of serial analysis of the extracellular domains of GHS receptor 1a. There are many methods for the analysis of ligand binding to and activation of receptors, such as mutation or photolabeling of the ligand or mutation of the receptor [17,18]. We have previously used mutagenesis methods to evaluate the motilin receptor, in the same subfamily of class A G protein-coupled receptor, and demonstrated the importance of the Cys residues and the perimembranous amino acids [19–21].

In the present study, we examined the predicted amino terminus and the first, second and third extracellular loops of the human GHS receptor 1a, and identified functionally important residues by using sequential deletions and site-directed alanine, phenylalanine, or aspartate replacement. Cys residues in positions 116 and 198 in the first and second extracellular loops and the perimembranous Glu^{187} residue in the second extracellular loop of this receptor were critical for biological activity of both natural peptide, ghrelin, and synthetic peptide, GHRP-6, same as the motilin receptor.

2. Materials and methods

2.1. Materials

Human ghrelin was from AnaSpec (Fremont, CA). GHRP-6 was from Peptide Institute, Inc. (Osaka, Japan). Protease-free cell dissociation buffer was from Sigma-Aldrich (Indianapolis, IN). Expression vector pcDNA3.1(−), Lipofectamine 2000, and 4′,6-diamidino-2-phenylindole (DAPI) were from Invitrogen (Carlsbad, CA). Enzymes used for receptor mutagenesis were purchased from Roche Applied Science (Tokyo, Japan) or Stratagene (La Jolla, CA). Fura-2 acetoxymethyl ester (AM) and Alexa555-conjugated goat anti-mouse IgG were from Molecular Probes (Eugene, OR). The mouse 12CA monoclonal antibody against the hemagglutinin (HA) epitope was from Roche Applied Science (Tokyo, Japan). 125-I-ghrelin was from PerkinElmer (Beaconsfield, UK). The human GHS receptor cDNA was kindly provided by Dr. Howard of Merck Research Laboratories (Rahway, NJ; Ref. [11]).

2.2. Receptor constructs

Constructs representing a series of mutations of the predicted extracellular domains of the human GHS receptor 1a were prepared (Fig. 1). There is the clear sequence homology between GHS and motilin receptor, particularly in the predicted transmembrane segments (86%). In the current study, we have set a schematic diagram of the predicted extracellular domains of the GHS receptor based on hydrophobicity of motilin receptor up [19,22]. This schematic diagram is slightly different from other reports by Holst et al. or Feighner et al. [23,24]. These represented deletions of segments ranging in length from one to twelve amino acid residues and substitutions of single amino acid residues in the perimembranous regions of interest with alanine or phenylalanine, the neutral amino acid, and aspartate, the similar charged amino acid to the original residues. Mutant GHS receptors were constructed by an oligonucleotide-directed approach. PCR was performed in a thermal cycler with Pfu Turbo DNA polymerase, running 18 cycles at 95 °C for 30 s, 65 °C for 1 min, and 68 °C for 14 min. Products of the PCR and

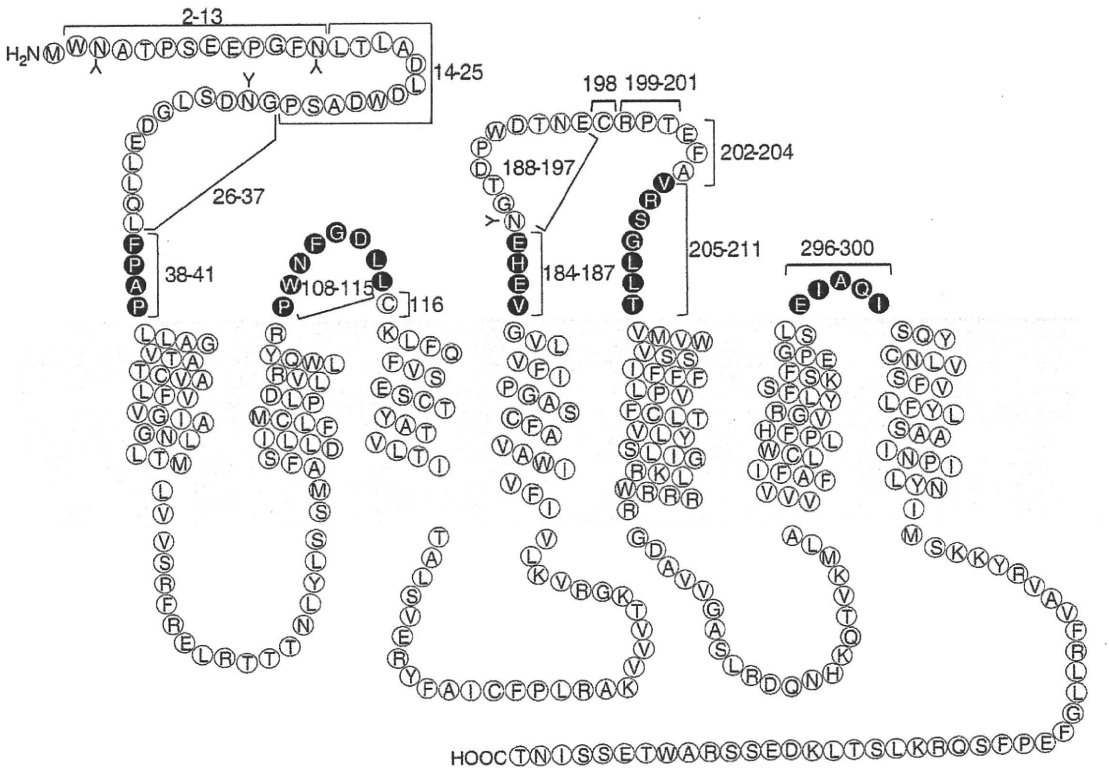

Fig. 1. Illustration of the human GHS receptor constructs used in this report. Shown is a schematic diagram of the primary sequence and a possible membrane topology (based on hydrophobicity) of the GHS receptor, along with the design of the sequential deletions (in numbered brackets) and Ala or Phe or Asp replacement constructs (in dark circles with white lettering).

restriction enzyme digestion were separated on 1% agarose gels and purified with a Qiagen kit (Valencia, CA). Receptor constructs were subcloned into pcDNA3.1(−). The sequences of all constructs were confirmed by direct DNA sequencing with an ABI Prism DNA Sequencer (Foster City, CA).

Additionally, a series of HA-tagged constructs were also prepared for immunostaining studies; these included HA-tagged wild-type, alanine site mutant (E187A), aspartate site mutant (E187D), and cystein deletion mutants (Δ116C and Δ198C). They were prepared using the same strategy as described above, by placing HA sequence (YPYDVPDYA) at the amino terminus between residues Met^1 and Trp^2 of the wild type or mutant receptors.

2.3. Receptor expression

Receptor constructs were expressed transiently in COS-1 cells (American Type Culture Collection), which do not naturally express the GHS receptor. Cells (1×10^5) plated on plastic culture ware were transfected with 1 μg of DNA using Lipofectamine 2000. Cells were cultured in Dulbecco's modified Eagle's medium with 5% fetal bovine serum. Cells were harvested with non-enzymatic cell dissociation solution 36 h after transfection for a biological activity assay and a radioligand binding assay.

2.4. Intracellular calcium biological activity assay

The abilities of each GHS receptor construct to respond to ghrelin and GHRP-6 were studied with a well-established assay for intracellular calcium signaling in fura-2 AM-loaded transfected COS cells. For this, COS cells expressing the receptor constructs were lifted with non-enzymatic cell dissociation solution, washed, and loaded with 5 μM fura-2 AM in serum-free culture medium by incubation at 37 °C for 20 min. Cells were then washed twice with Krebs–Ringer–HEPES (KRH) medium (in 25 mM HEPES, pH 7.4, 104 mM NaCl, 5 mM KCl, 1.2 mM $MgSO_4$, 1 mM KH_2PO_4, and 2 mM $CaCl_2$, with 0.2% bovine serum albumin and 0.01% soybean trypsin inhibitor) before being suspended in KRH medium at a density of 1.0×10^6/ml. Approximately 2.0×10^6 cells per assay were stimulated with varied concentrations of ghrelin and GHRP-6 at 37 °C, with fluorescence quantified in a PerkinElmer LS55 Luminescence Spectrometer (Beaconsfield, UK). Excitation was performed at both 340 nm and 380 nm, with emission determined at 520 nm and calcium concentration calculated from ratios as described by Grynkiewicz et al. [25]. The peak intracellular calcium concentration that was transiently achieved was used to determine the agonist concentration dependence of the biological responses. All assays were repeated at least four times.

2.5. Receptor binding assays

Radioligand binding assays were performed with the various GHS receptor-bearing cells, ^{125}I-labeled ghrelin (3–5 pM radioligand), and KRH medium. Incubations were carried out for 60 min at 25 °C, as previously described [20]. The binding assays were performed in 24-well tissue culture plates. Nonspecific binding was determined in the presence of 1 μM ghrelin and represented <20% of total binding. All assays were repeated at least four times.

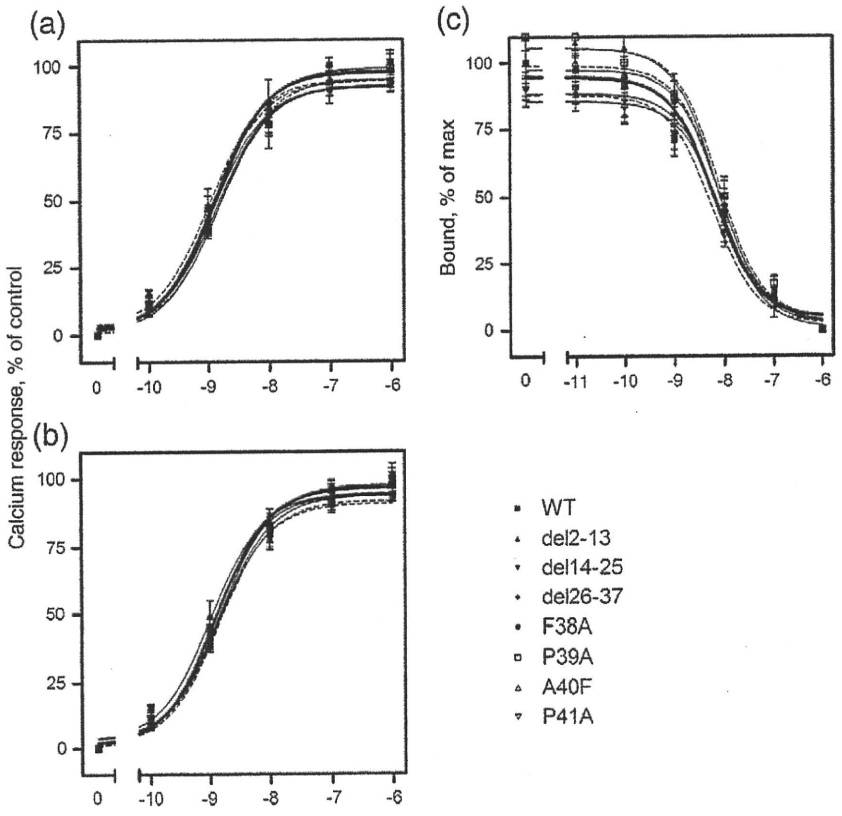

Fig. 2. Biological and binding activities of the GHS receptor amino-terminal constructs. Shown are intracellular calcium responses to increasing concentrations of ghrelin (a) and GHRP-6 (b) in COS cells transfected with deletion mutants and Ala or Phe replacement site mutants at the amino-terminus of the GHS receptor. Values are expressed as mean ± S.E. of data from four independent assays, with these values normalized relative to the maximal response to ghrelin and GHRP-6 in cells expressing the wild-type receptor (WT). Shown also is competition of ghrelin for binding of radioligand (^{125}I)-ghrelin to theses constructs expressed in COS cells (c). Values illustrated represent saturable binding as a percentage of competing ghrelin. All values are means ± S.E. of data from independent experiments.

2.6. Immunohistochemistry of GHS receptor

For morphological assessment of receptor expression on the cell surface, COS cells transiently transfected with HA-tagged wild-type or mutant GHS receptors were replaced to grow on coverslips for 36 h. Cells were washed with PBS and incubated with mouse monoclonal anti-HA antibody (1:500) for 30 min on living cells. After washes with PBC, cells were fixed in 2% paraformaldehyde for 30 min. After being washed with PBS, cells were incubated in Alexa555-conjugated goat anti-mouse IgG (1:400) for 1 h. Coverslips were then washed with PBS, and incubated with DAPI for 10 min for visualization of cell nucleus. All of the above procedures were performed at room temperature.

2.7. Statistical analysis

Biological activity curves and binding curves were analyzed and plotted using the nonlinear regression analysis program in the Prism software package (GraphPad Software, San Diego, CA). Binding kinetics was determined by analysis with the LIGAND program of Munson and Rodbard [26]. All results are expressed as means ± SE. Data were analyzed with a two-tailed, two-way analysis of variance followed by Newman–Keuls test to correct for multiple comparisons. A value of $p<0.05$ was regarded as significant.

3. Results

3.1. Mutagenesis of the amino terminus of the GHS receptor

In this series of studies, we sequentially deleted segments twelve amino acid residues in length between Trp^2 and Leu^{37} and replaced each of residues between Phe^{38} and Pro^{41} to Ala or Phe in the predicted amino-terminal tail region of the GHS receptor (Fig. 1). These started immediately after the initiator methionine residue. The constructs were transiently expressed in COS cells and were characterized functionally. As shown in Fig. 2 and Table 1, in all mutant constructs the intracellular calcium responses to ghrelin and GHRP-6 and binding capacity of radioactive ghrelin were similar to that in wild-type GHS receptor.

3.2. Mutagenesis of the first extracellular loop of the GHS receptor

In this region, we mutated each of eight residues between Pro^{108} and Leu^{115} to alanine and one deletion residue (Cys^{116}). The constructs were transiently expressed in COS cells and were functionally characterized. As shown in Fig. 3 and Table 1, of all mutated constructs, only Cys^{116} deletion mutant (Δ116C) demonstrated a significant reduction in ghrelin- and GHRP-6-stimulated intracellular calcium responses. Maximal calcium responses to ghrelin and GHRP-6 for this Δ116C mutant were only 10% of that for the wild-type GHS receptor. Consistent with this finding, Δ116C mutant exhibited low binding to radioligand ghrelin.

3.3. Mutagenesis of the second extracellular loop of the GHS receptor

In this region, we mutated each of four residues between Val^{184} and Glu^{187} to alanine, and each of seven residues between Val^{205} and Thr^{211} to alanine in the perimembranous regions. In addition, we sequentially deleted segments ranging in length from one to ten amino acid residues between Asn^{188} and Ala^{204}. Constructs were transiently expressed in COS cells and were characterized functionally. As shown in Fig. 4 and Table 1, only Cys^{198} deletion mutant (Δ198C) and Glu^{187} to Ala mutant (E187A) decreased the ghrelin- and GHRP-6-stimulated intracellular calcium responses relative to that in the wild-type receptor. The maximal calcium responses to ghrelin and GHRP-6 for this Δ198C and E187A were only 10–20% for that of the wild-type receptor. We constructed mutating Glu^{187} to Asp (E187D), which is negative-charge amino acid same as Glu, and tested. E187D mutant construct also decreased the intracellular calcium responses to ghrelin and GHRP-6. E187A, E187D, and Δ198C constructs also demonstrated low binding to radioactive ghrelin.

Table 1
Binding and biological activity data. Shown are the parameters of ghrelin binding to COS cells expressing each of the noted GHS receptor constructs. Shown also are EC_{50} values for ghrelin (nM)- and GHRP-6 (nM)-stimulated intracellular calcium responses in these cells, as well as E_{max} value reflecting maximal intracellular calcium concentrations (nM) achieved. All values are means ± S.E. of data from four independent experiments.

Receptor constructs	Ghrelin binding		Intracellular calcium response to ghrelin		Intracellular calcium response to GHRP-6	
	Ki (nM)	B_{max} binding sites/cells ($\times 10_3$)	EC_{50} [ghrelin] (nM)	E_{max} [Ca^{2+}] (nM)	EC_{50} [GHRP-6] (nM)	E_{max} [Ca^{2+}] (nM)
WT	6.2±2.1	94±18	1.2±0.3	30±6	1.2±0.4	34±7
Δ2-13	6.8±2.5	105±25	1.4±0.4	33±9	1.5±0.4	35±8
Δ14-25	8.4±2.8	88±19	1.3±0.2	29±5	1.2±0.2	32±5
Δ26-37	8.8±3.1	85±20	1.2±0.2	27±4	1.4±0.5	33±4
F38A	8.1±2.7	97±17	1.4±0.3	25±5	1.0±0.2	31±7
P39A	7.7±2.3	105±23	1.5±0.5	29±7	1.1±0.2	32±6
A40F	8.2±2.6	98±24	1.0±0.1	30±9	1.4±0.3	30±3
P41A	5.9±1.6	87±15	1.1±0.2	31±6	1.3±0.6	29±2
P108A	7.0±2.0	87±13	1.6±0.6	26±4	2.0±0.8	26±3
W109A	6.3±1.9	85±17	1.3±0.4	29±3	1.8±0.7	37±9
N110A	14.4±5.2	101±29	0.8±0.1	30±7	1.1±0.3	28±5
F111A	11.8±4,5	106±30	1.2±0.3	33±8	1.1±0.2	29±4
G112A	6.6±2.1	88±18	0.9±0.2	31±5	1.2±0.3	34±8
D113A	12.0±6.0	108±28	1.4±0.5	32±6	1.1±0.3	36±8
L114A	16.5±9.3	106±26	0.9±0.4	32±5	1.3±0.2	35±9
L115A	14.1±8.1	107±25	0.9±0.3	30±3	1.1±0.1	29±5
Δ116C	>1000		>1000	3±1	>1000	3±1
V184A	3.3±1.0	88±16	1.6±0.9	29±4	0.8±0.1	36±10
E185A	9.4±3.4	87±18	1.5±0.8	30±3	0.9±0.2	35±8
H186A	9.3±3.1	107±22	1.3±0.5	32±4	1.3±0.3	29±4
E187A	>1000		>1000	7±2	>1000	10±2
E187D	>1000		>1000	9±2	>1000	11±2
Δ188-197	6.6±2.9	88±12	1.4±0.5	33±7	1.4±0.5	28±
Δ198C	>1000		>1000	2±1	>1000	3±1
Δ199-201	6.3±1.7	85±17	1.6±0.7	31±7	1.3±0.3	25±3
Δ202-204	7.0±2.2	87±12	1.2±0.6	35±10	1.2±0.4	27±5
V205A	7.1±2.6	89±19	1.1±0.3	29±6	1.1±0.3	33±8
R206A	7.6±2.4	91±16	1.2±0.3	30±8	1.2±0.2	31±5
S207A	7.0±2.4	88±22	1.5±0.5	31±7	1.1±0.1	33±7
G208A	7.1±2.2	81±10	1.0±0.2	33±9	1.2±0.3	32±6
L209A	5.8±1.9	83±11	0.9±0.1	34±9	1.1±0.3	36±8
L210A	4.8±1.4	86±15	1.4±0.8	31±5	1.2±0.2	31±4
T211A	14.6±7.8	98±18	0.9±0.4	32±3	1.9±0.1	30±7
E296A	7.1±2.0	83±16	1.7±0.9	31±	0.9±0.1	32±9
I297A	8.0±2.6	108±21	1.2±0.7	32±	1.4±0.3	38±11
A298F	9.9±5.1	96±17	1.5±0.7	34±	0.8±0.1	34±8
Q299A	10.1±4.3	90±19	1.5±0.6	32±	0.9±0.1	31±7
L300A	5.7±1.8	85±21	1.4±0.4	31±	0.8±0.1	36±8

3.4. Mutagenesis of the third extracellular loop of the GHS receptor

This is a small region, consisting of five residues. We mutated each of five residues between Glu^{296} and Ile^{300} to Ala or Phe. As shown in Fig. 5 and Table 1, each residue mutant constructs resulted in similar intracellular calcium responses for both ghrelin and GHRP-6 stimulation to that in wild-type receptor. They also demonstrated same binding capacity to ghrelin as in wild-type receptor.

3.5. Evidence of surface expression of the functionally impaired mutant GHS receptor constructs

To examine cell surface expression of the functionally impaired GHS receptor constructs as identified above, each of the relevant HA-

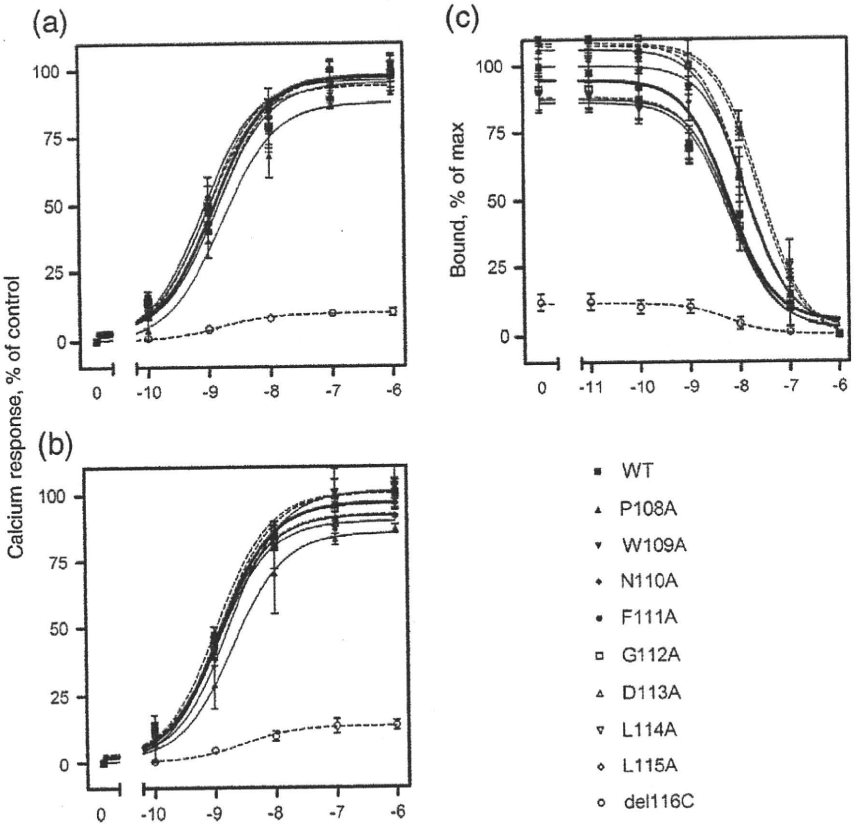

Fig. 3. Biological and binding activities of the GHS receptor first extracellular loop constructs. Shown are intracellular calcium responses to increasing concentrations of ghrelin (a) and GHRP-6 (b) in COS cells transfected with deletion mutant and Ala replacement site mutants at the first extracellular loop of the GHS receptor, as well as results from competition binding experiments (c). Data are illustrated as described in the legend for Fig. 2 from four independent experiments. WT, wild-type.

tagged constructs was transfected into COS cells and immunostained with anti-HA monoclonal antibody. As shown in Fig. 6, each mutant receptor construct was expressed on cell surface in density similar to the wild-type receptor. No fluorescence was observed in negative control cells that had been transfected with an empty expression vector or in cells transfected with wild-type receptor but stained with the second antibody only. It should be noted that the HA-tagged GHS receptor had ghrelin-stimulated biological activity responses similar to the wild-type receptor (data not shown).

4. Discussion

The motilin-growth hormone secretagogue family of receptors may follow unique and interesting molecular themes for binding and being activated by their natural ligands. This relates to the location of critical determinants for binding and biological activity at the amino-terminal ends of both motilin [22] and ghrelin [1] rather than at the carboxyl terminus, which is most typical of peptide receptors within the class A G protein-coupled receptors [27]. It is also possible that the members of this receptor family follow themes that are distinct even among themselves. This relates to the novel and functionally critical post-translational modification of ghrelin, n-octanoylation of Ser^3 [1], which is apparently absent in motilin. Such a modification could establish an association with the lipid bilayer that orients ghrelin in a unique manner prior to its receptor binding.

We previously reported that Cys residues and the perimembranous residues in the predicted extracellular loops and amino-terminal tail of the human motilin receptor are critical for natural peptide ligand, motilin, binding and biological activity [19,20]. To explore the possibility of distinct modes of binding for members of this receptor family, in this work, we focused our efforts on the predicted extracellular domains of the human GHS receptor 1a, and utilized receptor mutagenesis and intracellular calcium responses to systematically scan for residues that might be critical for ghrelin- and GHRP-6-stimulated biological responses. Three residues, Cys^{116} in the predicted first extracellular loop, Glu^{187} and Cys^{198} in the second extracellular loop were shown to be critical for calcium signaling, with each mutant affected similarly for stimulation by the natural peptide agonist ghrelin and the synthesized peptide agonist GHRP-6. Two Cys residues, Cys^{116} and Cys^{198}, within the predicted first and second extracellular loop domains are conserved throughout the class A superfamily of G protein-coupled receptors, and contribute to the formation of the highly conserved disulfide bond linking the first and second extracellular loop of these receptors [19,20]. The disulfide bond is necessary to maintain the structure of class A G protein-coupled receptor.

Although these data are of great interest and suggest the presence of a platform at the interface between the plasma membrane and extracellular domains for the natural peptide ghrelin binding to its receptor, these results are indirect and require complementation. Such loss-of-function studies can be explained by allosteric effects rather than as a site of direct ligand interaction with the receptor.

Our mutagenesis approach also revealed the new functional important perimembranous residue, Glu^{187}, in the predicted second extracellular loop domain, similar to the motilin receptor [19]. The molecular basis of ligand binding to a receptor is dependent on the structural and physiochemical characteristics of both molecules. For the superfamily of G protein-coupled receptors, the heptahelical structure and confluence of these helices in the lipid bilayer are

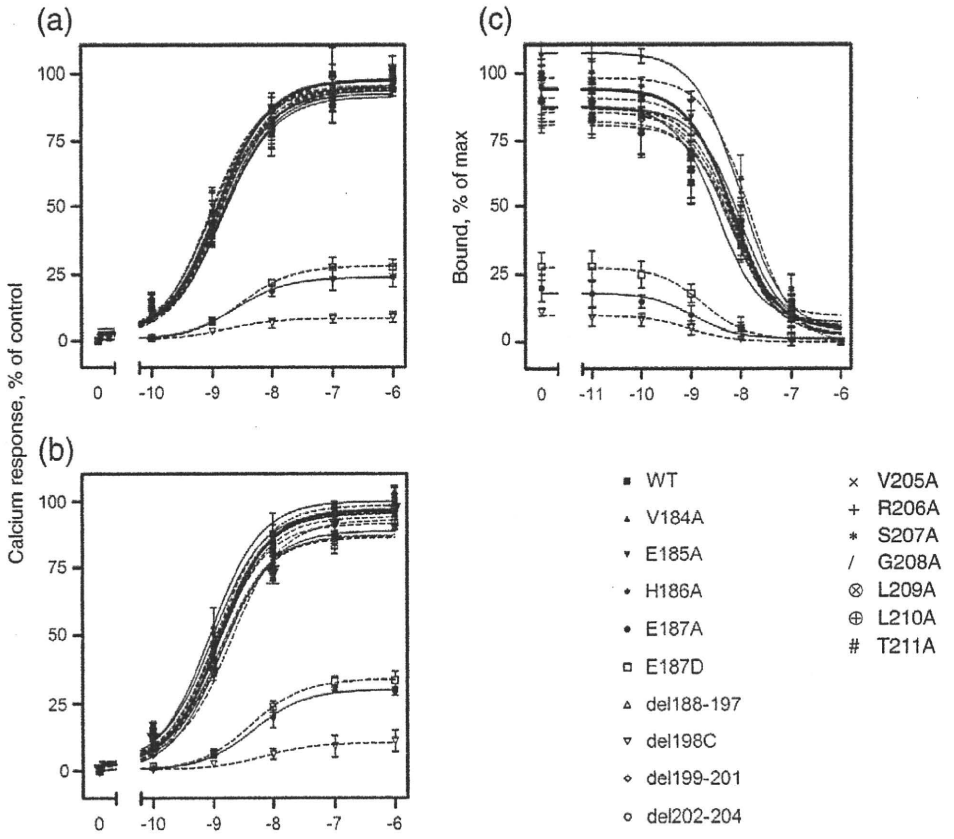

Fig. 4. Biological and binding activities of the GHS receptor second extracellular loop constructs. Shown are intracellular calcium responbses to increasing concentrations of ghrelin (a) and GHRP-6 (b) in COS cells transfected with deletion mutants and Ala or Phe or Asp replacement site mutants at the second extracellular loop of the GHS receptor, as well as competition binding data (c). Data are illustrated as described in the legend for Fig. 2 from four independent experiments. WT, wild-type.

thought to be largely conserved. However, the loop and tail regions are quite varied and likely provide the diversity of themes allowing the binding of structurally diverse natural ligands. Our present findings provide important new insights into the molecular basis of signaling at the GHS receptor.

The point mutation of the residue Ala^{204} to glutamate (A204E) in the second extracellular loop domain of human GHS receptor has been reported in patients with short stature [13,23,28]. In the current study, the binding capacity and intracellular calcium response to ghrelin in the deletion mutant receptor, including Ala^{204}, were similar to those of wild-type receptor. We have not examined the function of the replacement mutant receptor of residue Ala^{204} to any other amino acids in the present study. Holst et al. have reported that GHS receptor showed strong, ligand-independent signaling in transfected cells by measuring inositol phosphate turnover or by using a reporter assay for transcriptional activity, and ghrelin acted as agonist stimulating inositol phosphate turnover further and substance P acted full antagonist as it decreased the constitutive signaling of the GHS receptor. Pantel et al. have reported that the cell surface expression of A204E mutant receptor was decreased by means of HA-tagged construct, and the specific binding capacity to ghrelin of A204E receptor was about 20% of wild-type receptor. The high constitutive activity of GHS receptor was a key component of this receptor function in vivo, whereas A204E mutant receptor showed loss of function through a selective loss of constitutive activity for ligand response being preserved. In the present study, we have only evaluate ligand responses in vitro, so further investigation is necessary.

Expression of GHR receptor has been described not only in central nervous tissues but in peripheral tissues, including gastrointestinal tracts, liver, kidney, lung, myocardium, adipose tissue, placenta, and T cells [11,29–31]. The active sites of G protein-coupled receptors are of substantial interest for rational drug design. In this study, we demonstrated that Glu^{187} is an important residue for activation of the GHS receptor. If ghrelin agonists that bind to Glu^{187} strongly could be synthesized, new drug therapies may be developed for the treatment of various diseases, including appetite loss due to cancer and anorexia nervosa, short stature, chronic kidney disease, heart failure, and chronic obstructive pulmonary disease [5–10].

In conclusion, we have now demonstrated Cys residues in positions 116 and 198 in the first and second extracellular loops and the perimembranous Glu^{187} residue in the second extracellular loop of the GHS receptor were critical for ghrelin and GHRP-6 biological activity. These results suggest that Cys residues in the extracellular domains in this family of Class A G protein-coupled receptor is likely involved in the highly conserved and functionally important disulfide bond, and that the perimembranous residues contribute peptide ligand binding and signaling.

Acknowledgements

We thank Y. Yano for valuable contributions and cooperation. This work was supported by a grant (No. 20590727) from the Japanese Ministry of Education, Culture, Sports, Science and Technology.

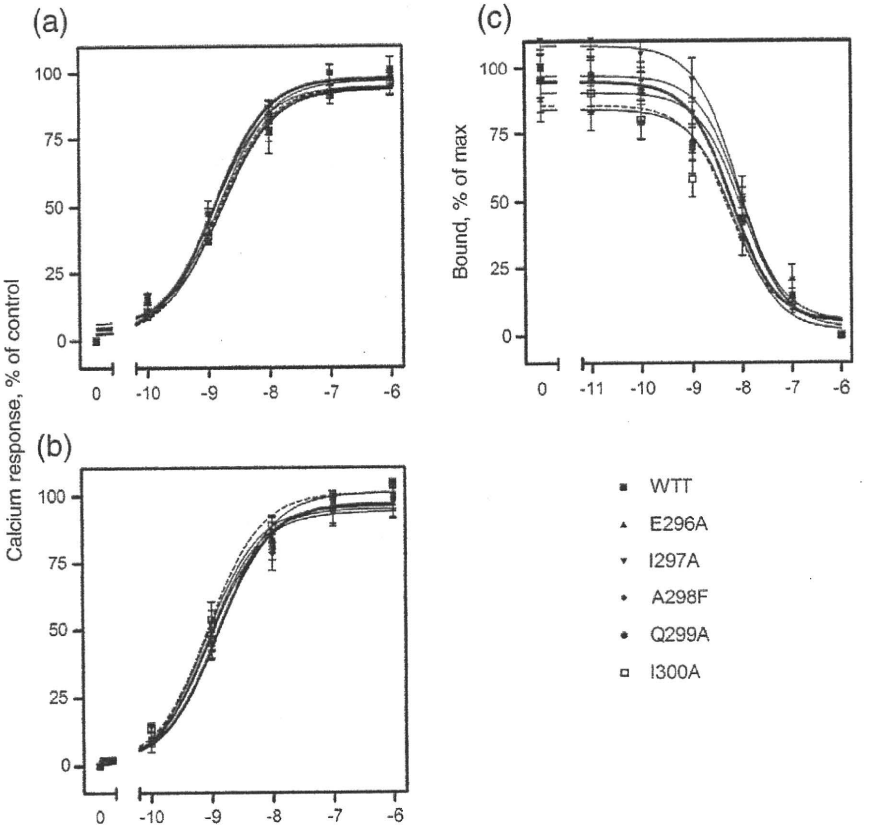

Fig. 5. Biological and binding activities of the GHS receptor third extracellular loop constructs. Shown are intracellular calcium responses to increasing concentrations of ghrelin (a) and GHRP-6 (b) in COS cells transfected with Ala or Phe replacement site mutants at the third extracellular loop of the GHS receptor, as well as competition binding data (c). Data are illustrated as described in the legend for Fig. 2 from four independent experiments. WT, wild-type.

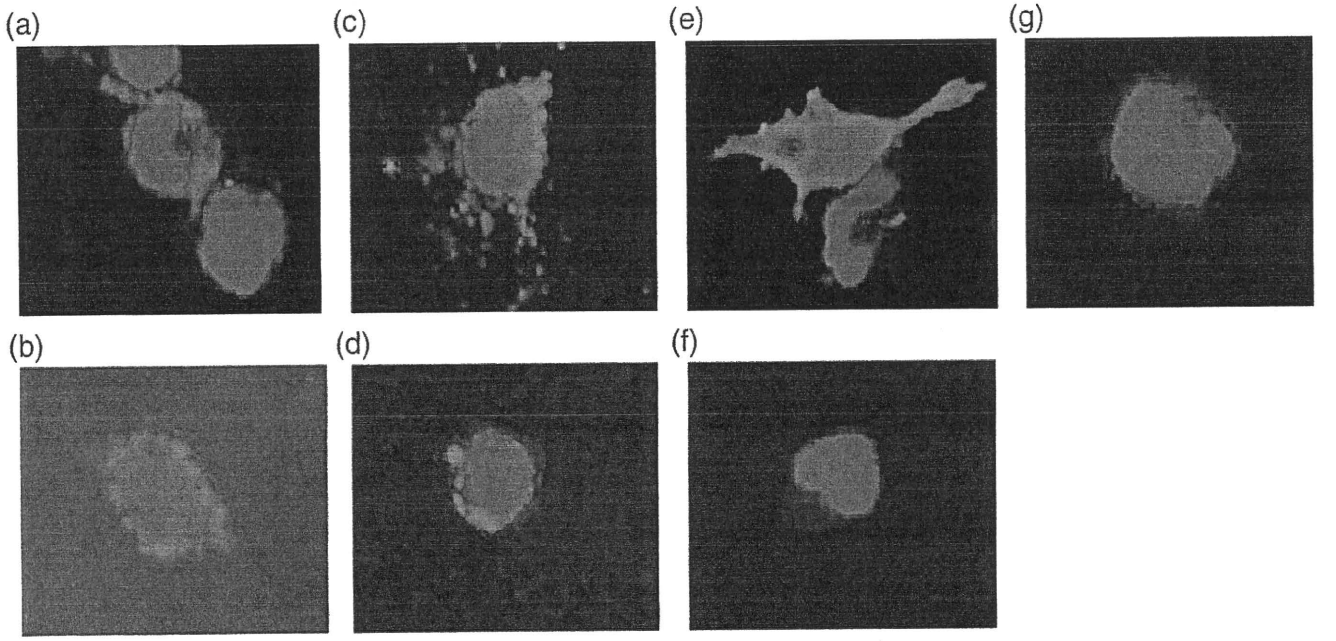

Fig. 6. Morphological evidence for normal cell surface expression of functionally impaired GHS receptor constructs. Shown are representative examples of anti-HA immunolabeling of COS cells transfected with HA-tagged wild-type (a), Δ116C (b), Δ198C (c), E187A (d), E187D (e) GHS receptor and cells transfected with the empty pcDNA3 eukaryotic expression vector (f). Shown also are COS cells transfected with HA-tagged wild-type GHS receptor but immunostained only with Alexa555-conjugated goat anti-mouse IgG (g). Cell nucleus was stained with 4′,6-diamidino-2-phenylindole (DAPI).